C. R. Mecanique 341 (2013) 421–428

Contents lists available at SciVerse ScienceDirect

Comptes Rendus Mecanique

www.sciencedirect.com

10th International Meeting on Thermodiffusion

In situ experimental observation of the time evolution of a dendritic mushy zone in a fixed temperature gradient

Georges Salloum Abou Jaoudé [a,b,*], Guillaume Reinhart [a,b], Henri Nguyen-Thi [a,b], Hervé Combeau [c], Miha Založnik [c], Thomas Schenk [c], Tamzin Lafford [d]

[a] *Aix-Marseille Université, campus Saint-Jérôme case 142, 13397 Marseille cedex 20, France*
[b] *CNRS, IM2NP UMR 7334, campus Saint-Jérôme case 142, 13397 Marseille cedex 20, France*
[c] *IJL, Département SI2M, UMR CNRS 7198, Lorraine University, École des mines de Nancy, parc de Saurupt, CS 14234, 54042 Nancy cedex, France*
[d] *European Synchrotron Radiation Facility (ESRF), 6, rue Jules-Horowitz, BP 220, 38048 Grenoble cedex 9, France*

ARTICLE INFO

Article history:
Available online 26 February 2013

Keywords:
Mushy zone
Solidification
Solid crust
Solute diffusion
Synchrotron
TGZM
X-ray radiography

ABSTRACT

This paper describes a series of experiments performed on BM05 at the European Synchrotron Radiation Facility (ESRF), dedicated to the analysis of a mushy zone evolution in a fixed temperature gradient. A mushy zone is the partially solid/partially liquid zone that is formed when solidification proceeds with the development of dendrites, and it has been recently shown that synchrotron X-ray radiography is a powerful technique, perfectly adapted for such a study. *In situ* and real-time characterisation clearly evidences the microstructural changes of the mushy zone during the holding stage, and measurements of the mushy zone boundary positions using image processing enable us to analyse the successive regimes. Each regime is directly related to solute diffusion mechanisms, namely temperature gradient zone melting, solute diffusion in the inter-dendritic liquid channels due to the solid-fraction gradient and solute diffusion in the melt.

1. Introduction

A mushy zone is the partially solid/liquid region that forms during directional solidification in a temperature gradient when solidification proceeds with the development of columnar dendrites (Fig. 1(a)). We will consider in this paper the case of an off-eutectic binary alloy that rejects its solute when the solid phase forms (i.e. partition coefficient lower than 1 and negative liquidus slope). In stationary conditions, the solid fraction g_S increases in the mushy zone (Fig. 1(b)) from zero at the dendrites tips (close to the liquidus temperature T_L of the alloy) to unity at the bottom of the mushy zone (at the solidus temperature T_S of the alloy) [1]. In addition to the imposed temperature gradient, a solute gradient is also caused by solute rejection during the growth process. The solute gradient in the vertical channels of the mushy zone is constant, which means that the liquid is close to the thermodynamic equilibrium [2]. Therefore, a complex coupling between thermal and solutal diffusion occurs inside and at the boundaries of this two-phase region. It is worth noticing that on earth, additional phenomena such as convection [3], sedimentation or floating of dendrite fragments [4] can increase the complexity of transport phenomena in the mushy zone. Most studies in solidification focused on the formation of the mushy zone and the determination of its main characteristics (shape and size), which are of great interest in many industrial applications because properties of the grown material are largely controlled by the microstructure(s) left in the solid during processing.

* Corresponding author at: Aix-Marseille Université, campus Saint-Jérôme case 142, 13397 Marseille cedex 20, France.
E-mail address: Georges.Salloum@im2np.fr (G. Salloum Abou Jaoudé).

1631-0721/$ – see front matter
http://dx.doi.org/10.1016/j.crme.2013.01.013

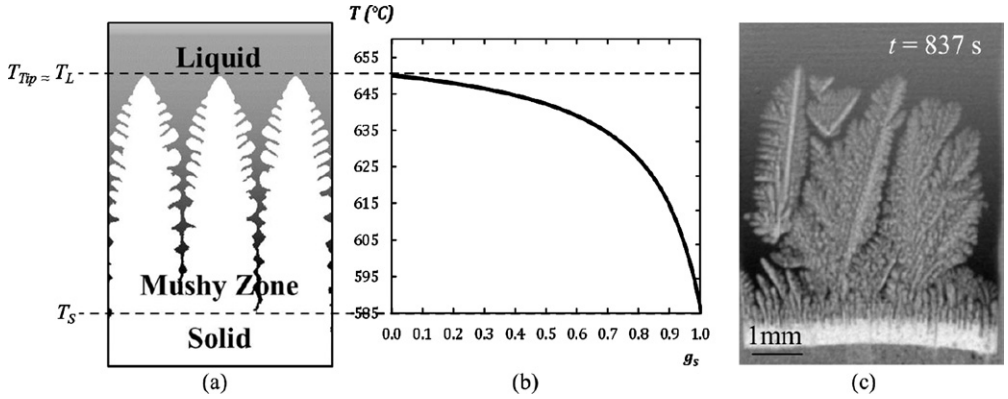

Fig. 1. (a) Schematic of the solid–liquid interface (mushy zone) during dendritic growth in stationary conditions. (b) Plot of the solid fraction g_S in the mushy zone calculated using the lever rule approximation. (c) Radiograph of an Al–4 wt% Cu sample during solidification, dendrites appear in white and the Cu-enriched liquid appears in dark grey.

The purpose of this work is quite different from these studies since we aim to investigate the evolution of a mushy zone in a fixed temperature gradient, *when solidification is stopped after formation of the mushy zone*. During this holding period (i.e. no modification of any experimental control parameters), several physical phenomena mainly controlled by diffusion can interact to dramatically change the microstructure of the mushy zone. First, reduction of the interfacial energy of the primary phase leads to a coarsening process or Ostwald ripening. In alloys, the coarsening process proceeds by the diffusion of mass from one region of the interface of high curvature to another of low curvature, which results in a more globular microstructure with a larger size scale. In addition, coalescence of dendrite arms can form liquid inclusions (droplet, channels) in the solid as recently observed in three-dimensional experimental analyses of coarsening phenomena of Al–Cu samples in isothermal conditions, conducted by Voorhees et al. by the serial sectioning technique [5] and by S. Terzi et al. using *in situ* tomography [6]. Second, due to the solute gradient in the liquid phase of the mushy zone, the solute diffuses from the bottom (cold side) to the top (hot side) of the mushy zone in the vertical liquid channels. This causes a slow solidification of the bottom of the mushy zone [7]. This solute diffusion is also responsible for the migration of liquid inclusions through a solid by temperature gradient zone melting (TGZM) [8,9]. Indeed, the opposite sides of the liquid inclusion are at different temperatures and therefore have a different solute composition as local thermodynamic equilibrium holds at the solid–liquid interface. Hence, there is a solute flux from the cold side to the hot side in the droplet, which causes solidification at the cold side and melting at the hot side so that the droplet migrates up the temperature gradient. TGZM plays a crucial role in the preparation of the initial conditions under which growth is started in directional-solidification experiments [8,9]. Third, H. Combeau et al. [10] recently showed that, in the presence of a gradient of solid fraction even with a fixed average solute gradient in the liquid phase, which is the case for a mushy zone, a non-zero net flux of solute induced by diffusion exists in the direction of the gradient of the liquid fraction (or in the opposite direction to the solid fraction gradient). This solute flux varies within the mushy zone proportionally with the liquid fraction. Thus the local variation of solute flux due to the gradient of liquid fraction induces a decrease of the local average concentration and solidification. By the way, solute diffusion in the liquid phase at the scale of the mushy zone is a driving force for a mushy zone to evolve towards a planar front and form a solid crust. It is worth noting that this effect is particularly efficient close to the dendrite tips, where the solid-fraction gradient is the largest.

Although this situation occurs in various important cases, such as severe accidents in nuclear reactors and the solidification of corium on its contact with the concrete walls [10], or the solidification of sea ice or magma chambers, few experimental or theoretical studies on this topic have been performed. A numerical model has been recently developed by Gewecke and Schulze [11] describing the evolution of a mushy zone formed during the solidification of a binary alloy cooled from below in a finite height tank. A rapid advance following by a slow retreat of the mushy zone was predicted but no experimental data are available to validate the model. The lack of experimental studies is probably due to the difficulty to obtain *in situ* and real-time information on the mushy zone characteristics, especially for metallic alloys. Classical analyses, such as quenching or decanting techniques, do not provide the interface evolution over time, but give only a “frozen” picture of the solid microstructure. To the best of our knowledge, no experimental study has been performed in metallic alloys, with *in situ* characterisation of the time evolution of mushy zone after stopping the solidification in a fixed temperature gradient. In the present work, the mushy zone was observed using synchrotron X-ray monitoring and further image processing was carried out to characterise its time evolution. In addition to qualitative observations on the microstructural changes, several main parameters were measured based on the radiographs, and their evolution is discussed.

2. Experimental procedures

2.1. Experiments

A series of four experiments were carried out on beamline BM05 at the ESRF (Grenoble, France) in a vertical Bridgman furnace [12]. Samples were prepared with a nominal composition of Al–4 wt% Cu. The sample size was 37 mm in length, 5 mm in width and 170–200 μm in thickness and was sandwiched between two graphite foils and two molybdenum diaphragms, held together with two molybdenum clips and fixed to a sample holder. The whole assembly was inserted vertically into a Bridgman furnace placed in an ultrahigh vacuum chamber.

The typical duration of an experiment was in the range 2–6 h; each experiment can be divided into two successive periods: the solidification and the holding stage. In the first stage, the sample was partially solidified to create a mushy zone. Solidification was induced by applying the power down method, with no displacement of the sample or the furnace. In this method, the temperatures of the hot and cold zones of the furnace were first adjusted to partially melt the sample (melting temperature $\approx 650\,^{\circ}\mathrm{C}$). For the experiments presented in this paper, the values for the hot and cold zones were roughly 680 °C and 620 °C respectively, and the desired temperature gradient G in the range 25–35 $\mathrm{K\,cm^{-1}}$. The temperature gradient along the crucible–sample set was measured by two embedded K-type thermocouples 2 cm apart, one close to the top-left and another close to the bottom-right of the sample. Then, solidification was triggered by applying a cooling rate ($R_{\mathrm{H}} = 1, 1.5$ or $2\ \mathrm{K\,min^{-1}}$) to the hot zone of the furnace while maintaining the cold zone temperature constant ($R_{\mathrm{C}} = 0$). In this technique, a slight decrease of the temperature gradient occurred during the solidification stage, typically about 1–2 $\mathrm{K\,cm^{-1}}$. The second stage of the experiment (i.e. the holding stage) was provoked when a sufficient mushy zone height was reached (approximately 2/3 of the height of the field of view). At this time, the cooling of the hot zone was stopped ($R_{\mathrm{H}} = 0$), and consequently the solidification. The holding stage began, with no modification of the heater temperatures, and thus with a fixed temperature gradient for the rest of the experiment.

For the experiments presented in this paper, the mushy zone evolution was observed using *in situ* X-ray monitoring. The main surface of the sample ($37 \times 5\ \mathrm{mm^2}$) was set perpendicular to the incident monochromatic X-ray beam at 13.5 keV. A Fast Readout–Low Noise (FReLoN) CCD camera developed at the ESRF was used as the detector and the camera optics were chosen so as to obtain a good compromise between a large field of view ($5.3 \times 8.3\ \mathrm{mm^2}$) and a satisfactory spatial resolution (pixel size $7.46 \times 7.46\ \mu\mathrm{m^2}$). Successive images of the solid–liquid zone were recorded at a maximum frequency of about 0.3 Hz and it was thus possible to display videos (image sequences) of the mushy zone evolution. The as-recorded or raw radiographs always presented several spurious artefacts due to the non-uniform profile of the X-ray beam, monochromator defects or surface defects on the crucible. These artefacts may considerably reduce image clarity and prevent quantitative analysis; therefore image processing was applied to improve the radiograph quality. It consisted in dividing the as-recorded image of the sample taken at a time t by a reference image recorded at an initial time t_0 before solidification was started, when most of the sample was liquid [13]. A radiograph of the mushy zone at the end of the solidification stage during a typical experiment is shown in Fig. 1(c), where solid dendrites appear in white while Cu-enriched liquid is in dark grey. It is worth noting that, owing to our experimental procedure, the solidification took place in transient conditions. Consequently, the mushy zone visible in Fig. 1(c) can present differences compared to the ideal stationary case of Fig. 1(a). Furthermore, local solute enrichment in the melt notably in the mushy zone is visible by variation of grey levels, in particular just above the solid–liquid interface.

2.2. Quantitative image processing

Based on the radiographs, two key parameters of the mushy zone were determined and analysed as a function of time (Fig. 2(a)), namely i) the highest position of the mush–liquid interface, noted Z_{ML}, and ii) the average position of the top of

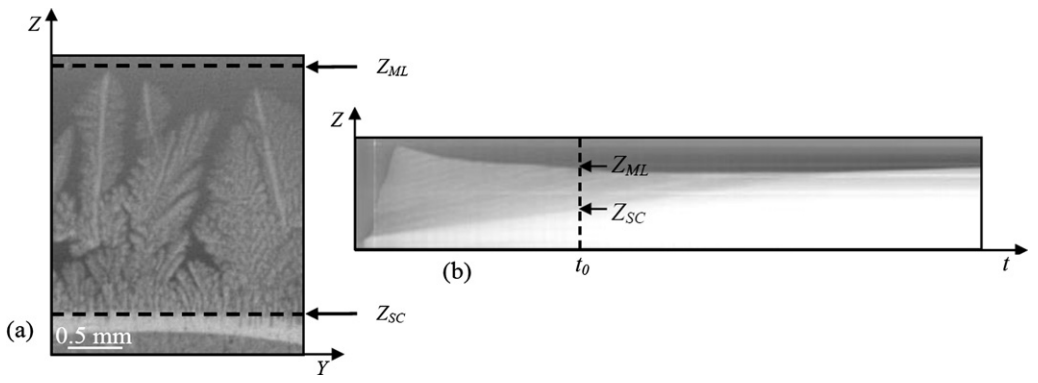

Fig. 2. (a) Image of Al–4 wt% Cu sample at an arbitrary time t_0 during solidification showing the mushy zone with the mush–liquid (at the top) and solid crust (at the bottom) interfaces. (b) Mushy zone boundaries as a function of time.

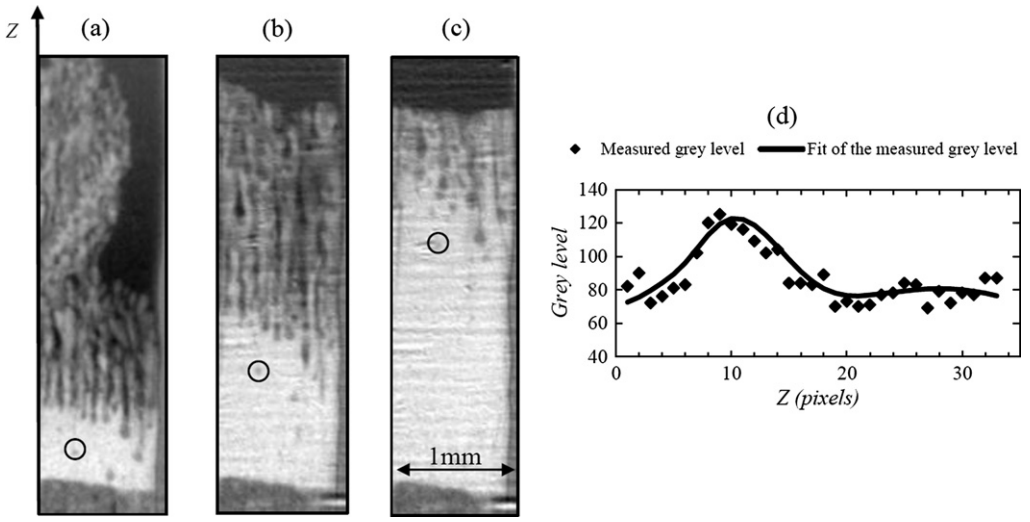

Fig. 3. ((a), (b), (c)) Radiographs showing an enriched Cu liquid droplet migrating towards the top of the mushy zone due to TGZM. (d) Plot of the grey level profile through the droplet in the Z-direction.

the solid crust that forms at the base of the mushy zone, noted Z_{SC}. These two parameters were measured for each image by a home-made image analysis method using ImageJ (website: http://rsb.info.nih.gov/ij/). First, the average value of the pixel intensity along the horizontal direction (Y-axis) was calculated as a function of the vertical direction (Z-axis) for each image of the experiment (see Fig. 2(a) for the axis orientation). These profiles were thus plotted to visualise the evolution of the mushy zone boundaries as a function of time (Fig. 2(b)) and measurements (± 15 μm) of Z_{ML} and Z_{SC} were achieved by applying two different thresholds, followed by a polynomial fit of the experimental curves.

During the experiment, droplet migration due to TGZM [8,9] was also observed (Figs. 3(a) to 3(c)). Migration velocities for selected liquid droplets were measured using a home-made image analysis method. The centre of the droplet was first automatically determined by plotting a grey level profile through the droplet in the Z-direction (Fig. 3(c)). This profile enabled us to determine the value of the centre of the bump which corresponds to the middle of the droplet. It was then possible to follow the position of a droplet as a function of time and then to deduce the droplet velocity.

3. Experimental results

3.1. Microstructural changes of the mushy zone

Similar conclusions could be drawn from all experiments. Therefore for the sake of clarity we focus in this paper on one typical experiment of an Al–4 wt% Cu sample, for which solidification was triggered by applying a cooling rate on the hot zone of the furnace $R_H = 2.5\ \mathrm{K\,min^{-1}}$ while maintaining the cold zone temperature constant ($R_C = 0$). Fig. 4 shows the microstructural changes during this experiment. The directional solidification stage occurred for $t \leqslant 837$ s. First, the growth of a planar front was observed for $t \leqslant 175$ s (Fig. 4(a)), then planar interface breakdown occurred and the dendritic front developed, leading to the formation of the mushy zone. The origin of the breakdown of the planar interface is understood in the light of constitutional undercooling of the melt ahead of the solid–liquid interface [14]. The macroscopic modulation of the solidification front and the local Cu-enrichment on both sides of the sample in Fig. 4(b) is due to convection arising from residual transverse temperature gradients. Indeed, even in a stable thermal–solutal configuration (vertical upward solidification, with a rejected solute denser than the solvent) convection is unavoidable during solidification on earth. A thoroughly analysis was recently conducted by Bogno et al. [2] about the convection effects on the dynamic evolution of the solid–liquid interface and on solute distribution during the initial transient of solidification, using the same experimental set-up. Moreover, nucleation and growth of an equi-axed grain is also visible on the left side of the sample, where Cu-enrichment increased the solutal undercooling ($t = 491$ s). At $t = 837$ s, the cooling of the hot heater (i.e. the solidification) was stopped. From this time on and until the end of the experiment, the temperature gradient was maintained fixed at $30 \pm 1\ \mathrm{K\,cm^{-1}}$. The dendrite tips reached a maximum position ($Z_{ML} = 5400$ μm) and the holding phase started.

Immediately after the end of the solidification phase, a slow retreat of the mush–liquid interface is visible concomitantly with the advance of the solid crust (Fig. 4(d)). For $t = 4402$ s (Fig. 4(e)), the dendritic morphology disappeared. No evidence of the initially dendritic microstructure is visible and only vertical channels and droplets remain. Z_{ML} continues to decrease until reaching a minimum position at $t = 7538$ s ($Z_{ML(min)} = 4050$ μm), while the solid crust interface continues to advance (Fig. 4(f)). At $t = 10\,652$ s, a merging of the mush–liquid and the solid crust interfaces occurred and a continuous advance of the resulting solid–liquid interface is observed, with some remaining liquid droplets and vertical channels (Fig. 4(g)). The experiment was stopped at $t = 11\,200$ s, for a solid crust position at 4237 μm (Fig. 4(h)).

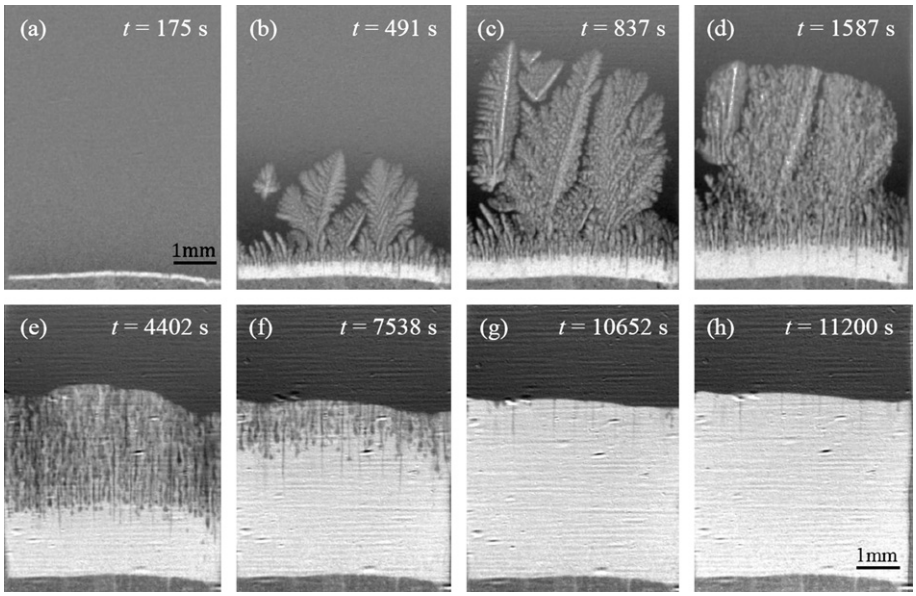

Fig. 4. Sequence of radiographs showing the microstructural changes of the mushy zone during the experiment for different times (a) planar front solidification. (b) Mushy zone formation during dendritic solidification. (c) Mushy zone at the end of solidification. ((d), (e), (f)) Radiographs showing the retreat of the mush–liquid interface with the advance of the solid crust. (g) Merging of the mush–liquid and the solid crust interfaces with some remaining liquid droplets and vertical channels. (h) Radiograph showing a continuous advance of the solid–liquid interface.

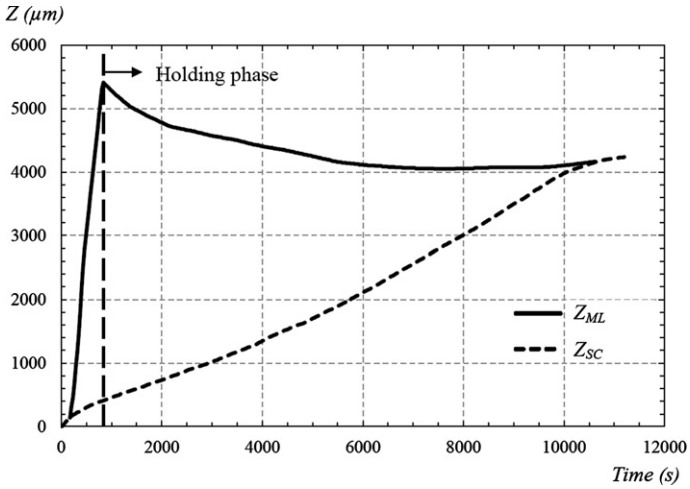

Fig. 5. Plots showing the variation of the position of the mush–liquid Z_{ML} and the solid crust Z_{SC} interfaces during the whole experiment (solidification and holding phase). Measurements are made by image processing of radiographs.

3.2. Variations of the mushy zone boundaries

Using the image treatment technique described in the experimental procedure, the mushy zone and solid crust positions were measured and plotted for the whole duration of the experiment (Fig. 5). The successive steps of the experiment were precisely defined, namely the solidification phase, the simultaneous decrease of Z_{ML} and increase of Z_{SC} before their junction and finally the slow motion of the interface towards the hot part of the sample. This figure is in excellent qualitative agreement with calculations recently conducted by Gewecke and Schulze [11], who investigated the evolution of a mushy zone in purely diffusive conditions.

For Z_{ML}, the top of the mush–liquid interface, three main different regimes are visible (Fig. 5, plain line). The first regime ($t \leqslant 837$ s) shows a very fast increase of Z_{ML} up to a maximum $Z_{ML(max)} \approx 5400$ μm and corresponds to the mushy zone formation undergoing the Mullins–Sekerka instability [14]. The maximum position can be defined as the end of the solidification phase. Then, a gradual retreat of the mushy zone takes place (837 s $\leqslant t \leqslant$ 7538 s), with first a fast decrease of the retreat velocity (from $V_{ML} = 0.7\ \mu m\,s^{-1}$ to $0.24\ \mu m\,s^{-1}$ for 837 s $\leqslant t \leqslant$ 2400 s) and then a much slower velocity (from $V_{ML} = 0.24\ \mu m\,s^{-1}$ to $0\ \mu m\,s^{-1}$ for a longer period 2400 s $\leqslant t \leqslant$ 7538 s). At $t = 7538$ s, a minimum position

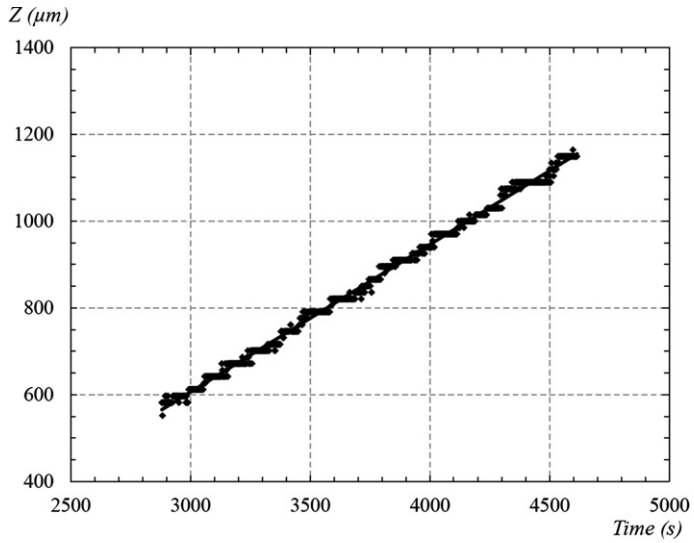

Fig. 6. Variation of the droplet position as a function of time during the holding phase induced by TGZM. Measurements are made by image processing of radiographs. The slope of the linear fit gives the droplet migration velocity, about 0.34 $\mu m\,s^{-1}$.

$Z_{ML(min)} \approx 4050$ μm is reached, which means that a total height of ≈ 1350 μm was melted from the initial mushy zone. The third and last regime for the mush–liquid interface (7538 s $< t <$ 10 652 s) corresponds to a very slow regrowth (with $V_{ML} = 0\ \mu m\,s^{-1}$ to $V_{ML} = 0.06\ \mu m\,s^{-1}$), until the merging of the mush–liquid and the solid crust interfaces.

For the solid crust's evolution, three different regimes are also detected (Fig. 5, dashed line). The first regime (0 s $\leqslant t \leqslant$ 175 s) corresponds to the initial planar front solidification, with an approximate growth velocity of $V_{SC} = 0.82\ \mu m\,s^{-1}$. The second regime (175 s $\leqslant t \leqslant$ 10 652 s) is a long and slow quasi-steady growth, with an increase in mean velocity V_{SC} (from 0.29 $\mu m\,s^{-1}$ for 175 s $\leqslant t \leqslant$ 3850 s to 0.39 $\mu m\,s^{-1}$ for 3850 s $\leqslant t \leqslant$ 6700 s and to $V_{SC} = 0.47\ \mu m\,s^{-1}$ for 6700 s $\leqslant t \leqslant$ 10 625 s). Finally, the third regime occurs after the merging of the mush–liquid and the solid crust interfaces at $t =$ 10 652 s, with a mean growth velocity of 0.13 $\mu m\,s^{-1}$.

Several liquid droplets formed inside the mushy zone due to coarsening of the microstructure. The migration of several liquid droplets is observed in the whole area of the sample, through the solid aluminium phase and towards the hot part of the sample. By using the image treatment method described in the experimental procedure, the position curve of several droplets can be measured. Fig. 6 is a typical measurement, and it shows a quasi-linear variation with a migration velocity $V_{mig} = 0.34\ \mu m\,s^{-1}$ for 3000 s $\leqslant t \leqslant$ 4600 s. This value is of the same order of magnitude as the migration velocity of liquid droplets by TGZM found in Al–Ni alloys (0.3 $\mu m\,s^{-1}$) [9]. Similar measurements made at different time intervals during the experiment showed that the migration velocity of the droplets slowly increases as a function of time (from 0.30 to 0.34 $\mu m\,s^{-1}$). This increase is probably due to the decrease in solute concentration inside the droplets as they come near the solid–liquid interface as expected from the phase diagram. It is worth noting that the migration velocities of droplets and the solid crust are of the same order of magnitude and follow the same behaviour. This observation suggests that the driving force for the solid crust motion can also be related to the TGZM physical mechanism.

4. Discussion

In situ measurements of the present investigation enable us to precisely define the successive steps in the time evolution of the mushy zone during the holding phase. After the solidification phase, one of the key features is the reduction of the mushy zone length on both sides: a retreat of the mush–liquid interface at the top of the mushy zone concomitantly with a slow growth of the solid crust at the bottom of the mushy zone (Figs. 4 and 5). After a sufficiently long time, the two interfaces merge, eliminating the mushy zone and forming a solid crust growing slowly.

The motion of the two interfaces leading to the mushy zone shrinking is mainly caused by solute diffusion inside and outside the mushy zone as predicted by N.R. Gewecke and T.P. Schulze [11]. Solute transport induces melting at the top of the mushy zone and solidification inside and at the bottom of the mushy zone. Assuming that the liquid stays in full thermodynamic equilibrium during the whole duration of the holding stage and that convection is negligible during the holding stage, a uniform solute flux density in the Z-direction equal to the ratio of the thermal gradient by the liquidus slope time the solute diffusion coefficient will remain. This solute flux density induces a solidification progressing from the bottom of the mush with a planar front. On the other hand, inside the mush, the net flux of solute in the direction of the thermal gradient (Z-direction) corresponding to the transport by diffusion varies with the height as it is proportional to the liquid fraction. This variation of the flux also induces a local variation of the average concentration and solidification as pointed out by Combeau et al. in [10]. The solidification induced by the gradient of the liquid fraction is more effective

close to the dendrite tips, where the gradient of the liquid fraction is the largest. For this reason, in the early stages of the holding phase, only a slow solidification is observed at the bottom of the mushy zone whereas solidification is clearly visible at the top. In addition to these two effects, coarsening phenomenon also happens which can modify the mushy zone morphology, in particular by inducing dendrite fragmentation or closing of some liquid channels. However, as shown by other experiments that will be published in the future, these additional phenomena do not drastically change the general conclusions. The cumulative action of the two diffusion processes induces a fast retreat of the mush–liquid interface at a rate of 0.7 $\mu m\,s^{-1}$ due to solute accumulation at the mush–liquid interface (Figs. 4(c) and 4(d)) locally decreasing the equilibrium temperature. As the gradual disappearance of vertical liquid channels proceeds (Figs. 4(d) to 4(f)) the mush–liquid retreat velocity decreases down to 0.24 $\mu m\,s^{-1}$. It is worth noting that at the beginning of the holding stage, the dendrite spacing (Fig. 2(a)) is comparable to the sample thickness 170–200 μm and one can expect strong effects of sample confinement. Therefore, quantitative difference of the solid-fraction profile and rate of the mushy zone shrinking may be expected, compared to the 3D configuration. After approximately $t = 2000$ s, the large horizontal scale of the fine structure completely disappears (Figs. 4(d) and 4(e)) and only the scales below 0.1 mm, corresponding to the liquid inclusions formed by coarsening, persist. The size of these inclusions is significantly smaller than the sample thickness and hence the situation becomes similar to the 3D case. The droplet migration velocity due to TGZM we report is therefore the same as it would be in 3D. This transition from a confined to a 3D configuration could influence the slope of the mush–liquid interface position after $t = 2000$ s and change the slowdown dynamic compared to the one predicted in theoretical work [11].

For the subsequent regime (started at $t = 7538$ s and ended at $t = 10\,652$ s), the solid crust continues to advance while the mush–liquid interface experiences a very slow regrowth, with a velocity increase from $V_{ML} = 0\ \mu m\,s^{-1}$ to $0.06\ \mu m\,s^{-1}$. This behaviour is due to a change of the net flux at the mush–liquid interface. Indeed, due to the solute accumulation at the mush–liquid, a solute gradient in the liquid phase progressively forms, which gives birth to a solute flux in the bulk liquid phase [9]. In the previous regime, this liquid flux is negligible comparing to the solute flux coming from the mushy zone. However, in the present regime, since the latter tends towards zero, the liquid flux effect gains in importance and more solute is transported into the bulk liquid. The Cu concentration in the liquid ahead of the mushy zone then decreases, leading to a regrowth at the mush–liquid interface before the merging with the solid crust interface.

Finally, the third and last phase takes place after the merging of the two mushy zone interfaces at $t = 10\,652$ s, which means that there is no mushy zone any more (Fig. 4(g)). The solid–liquid interface continues to advance with a mean growth velocity of $0.13\ \mu m\,s^{-1}$ due to the solute transport in the liquid phase. The velocity is faster than in the previous regime since the solute flux coming from the mushy zone has disappeared. The diffusion of Cu into the bulk increases the equilibrium temperature of the solid–liquid interface and causes the growth of the solid crust. In addition to diffusion transport, some solute mixing in the liquid phase can also be provoked by convection, owing to the presence of a residual transverse temperature gradient as indicated by the slight curvature of the interface. Further analyses need to be performed in order to evaluate the contribution of each mechanism to the total solute flow in this regime.

5. Conclusion

In situ observation using X-ray imaging at the third-generation synchrotron radiation source of the ESRF allowed us to study the influence of solute diffusion on the evolution of the mushy zone during stabilisation in a fixed temperature gradient. Different regimes are identified and precisely characterised. In a first step, the cumulative action of all diffusion phenomena leads to a fast reduction of the mushy zone length on both sides. In a second step, TGZM is the dominant mechanism and the last regime is controlled by solute diffusion in the liquid phase only.

Further analyses are in progress, such as microprobe measurements, and complementary experiments on a different alloy with a smaller solidification interval (Al–Ni) are under analysis. These experimental results will allow us to develop and adapt numerical models dedicated to this topic.

Acknowledgements

The authors gratefully acknowledge all their colleagues at IM2NP (especially Dr. A. Bogno), IJL and the ESRF, Grenoble, who participated to the synchrotron experimental campaigns; without them this paper could not have been written. The authors wish to thank the ESRF for providing beam time under experiment code MA1277, and all staff members of the BM05 beamline for their technical support.

References

[1] D.A. Porter, K.E. Easterling, Phase Transformations in Metals and Alloys, Chapman & Hall, London, UK, 1992.
[2] A. Bogno, H. Nguyen-Thi, A. Buffet, G. Reinhart, B. Billia, N. Mangelinck-Noël, N. Bergeon, J. Baruchel, T. Schenk, Analysis by synchrotron X-ray radiography of convection effects on the dynamic evolution of the solid–liquid interface and on solute distribution during the initial transient of solidification, Acta Mater. 59 (2011) 4356–4365.
[3] M.G. Worster, The dynamics of mushy layers, J. Fluid Mech. 237 (1992) 649–669.
[4] H. Nguyen-Thi, A. Bogno, G. Reinhart, B. Billia, R.H. Mathiesen, G. Zimmermann, Y. Houltz, K. Loth, D. Voss, A. Verga, F. de Pascale, Investigation of gravity effects on solidification of binary alloys with in situ X-ray radiography on earth and in microgravity environment, in: A. Meyer, I. Egry (Eds.), International Symposium on Physical Sciences in Space, IOP Publishing Ltd., Bristol, 2011.

[5] J.L. Fife, P.W. Voorhees, The morphological evolution of equiaxed dendritic microstructures during coarsening, Acta Mater. 57 (2009) 2418–2428.
[6] S. Terzi, L. Salvo, M. Suery, A.K. Dahle, E. Boller, Coarsening mechanisms in a dendritic Al–10% Cu alloy, Acta Mater. 58 (2010) 20–30.
[7] M. Buchmann, M. Rettenmayr, Microstructure evolution during melting and resolidification in a temperature gradient, J. Cryst. Growth 284 (2005) 544–553.
[8] H. Nguyen Thi, B. Drevet, J.M. Debierre, D. Camel, Y. Dabo, B. Billia, Preparation of the initial solid–liquid interface and melt in directional solidification, J. Cryst. Growth 253 (2003) 539–548.
[9] H. Nguyen Thi, G. Reinhart, A. Buffet, T. Schenk, N. Mangelinck, H. Jung, N. Bergeon, B. Billia, H. Härtwig, J. Baruchel, In situ and real-time analysis of TGZM phenomena by synchrotron X-ray radiography, J. Cryst. Growth 310 (2008) 2906–2914.
[10] H. Combeau, B. Appolaire, J.-M. Seiler, Interface temperature between solid and liquid corium in severe accident situations: A comprehensive study of characteristic time delay needed for reaching liquidus temperature, Nucl. Eng. Des. 240 (2010) 1975–1985.
[11] N.R. Gewecke, T.P. Schulze, The rapid advance and slow retreat of a mushy zone, J. Fluid Mech. 674 (2011) 227–243.
[12] A. Buffet, G. Reinhart, T. Schenk, H. Nguyen-Thi, J. Gastaldi, N. Mangelinck-Noël, H. Jung, J. Härtwig, J. Baruchel, B. Billia, Real-time and in situ solidification of Al-based alloys investigated by synchrotron radiation: a unique experimental set-up combining radiography and topography techniques, Phys. Status Solidi A 204 (2007) 2503.
[13] A. Buffet, H. Nguyen Thi, A. Bogno, T. Schenk, N. Mangelinck-Noël, G. Reinhart, N. Bergeon, B. Billia, J. Baruchel, Measurement of solute profiles by means of synchrotron X-ray radiography during directional solidification of Al–4 wt% Cu alloys, Mater. Sci. Forum 649 (2010) 331–336.
[14] W.W. Mullins, R.F. Sekerka, Stability of a planar interface during solidification of a dilute binary alloy, J. Appl. Phys. 35 (1964) 444.